Spectral properties of Shiba subgap states at finite temperatures

Rok Žitko

Jožef Stefan Institute, Jamova 39, SI-1000 Ljubljana, Slovenia
and Faculty of Mathematics and Physics, University of Ljubljana, Jadranska 19, SI-1000 Ljubljana, Slovenia

Using the numerical renormalization group (NRG), we analyze the temperature dependence of the spectral function of a magnetic impurity described by the single-impurity Anderson model with a superconducting host. With increasing temperature the spectral weight is gradually transferred from the δ peak to the continuous subgap background, and both spectral features coexist at finite temperatures: the δ peak persists to temperatures of order Δ. The continuous background is due to inelastic exchange scattering of Bogoliubov quasiparticles off the impurity, and it is thermally activated since it requires a finite thermal population of quasiparticles above the gap. In the singlet regime for strong hybridization or away from the particle-hole symmetric point (charge-fluctuation regime) an additional subgap structure is observed just below the gap edges. It has thermally activated behavior with an activation energy equal to the Shiba state excitation energy.

I. INTRODUCTION

A magnetic impurity in a superconducting host induces localized bound states inside the spectral gap, known in different communities as either Shiba, Yu-Shiba-Rusinov, or Andreev bound states [1–10]. At zero temperature, Shiba states manifest as pairs of δ-peak resonances in the impurity spectral function $A(\omega)$ positioned symmetrically at positive and negative frequencies corresponding to the transitions from the many-particle ground state to the *same* many-particle excited state by either adding a probing electron to the system ($\omega > 0$) or removing it ($\omega < 0$). The intrinsic temperature dependence of the spectral function depends on the impurity dynamics. When the impurity behaves as a classical object, i.e., as a local magnetic field which is perfectly *static* on the time scale of the experiment ("adiabatic limit" with no dynamics of the internal degrees of freedom of the impurity), the corresponding *classical* impurity model is a quadratic noninteracting Hamiltonian; hence the spectral function is not temperature dependent at all. This problem can be discussed in terms of single-particle levels and their occupancy. When the impurity behaves, however, as a quantum object, i.e., a *fluctuating* local moment as described by the Kondo or Anderson *quantum* impurity models, there will be nontrivial intrinsic temperature dependence due to electron-electron interactions (inelastic exchange scattering of thermally excited Bogoliubov quasiparticles off the impurity spin). This problem is better addressed from the perspective of many-particle eigenstates. Since the eigenvalue spectrum of the Hamiltonian operator includes both discrete subgap states and a continuum part above the gap, it is expected that there will be both δ peaks and a continuous background coexisting inside the gap at any finite temperature, providing a further realization of the "bound state in the continuum" paradigm.

There are only few experimental works where the temperature dependence of the transport properties of the impurity systems in the subgap region has been discussed. The strong temperature effects found in the differential conductance in carbon nanotube quantum dots were accounted for using the tunneling formalism without the need for invoking any intrinsic temperature dependence of the impurity spectral function itself [11]. The most notable effect was the reversal of the curvature in the secondary spectral features which can be explained through the thermal occupation of the excited subgap states. Another experimental realization of impurity models is magnetic adatoms on superconducting surfaces. In Ref. [12] the measured differential conductance at two different temperatures was discussed in terms of a phenomenological impurity model based on a classical impurity with the relaxation dynamics described as an extrinsic process. For weak tip-sample tunneling, the relaxation rates associated with the adatom-substrate coupling are faster than the tip-substrate tunneling, and the current is dominated by the single-particle current. For stronger tip-sample tunneling, the tunneling rates are comparable to or larger than the adatom-substrate relaxation, and the Andreev current becomes important.

While the *position* and *weight* of the Andreev states inside the gap can be easily extracted from both the experimental differential conductance (dI/dV spectrum) and the computed impurity spectral function (imaginary part of the Green's function) and compared to validate theoretical models [7,13–15], it is much more difficult to reliably deconvolve the differential conductance with the aim of extracting the impurity spectral function and studying the detailed distribution of the spectral weight within the gap, in particular the *width*. The primary reason is that there are multiple processes contributing to transport (primarily single-particle tunneling and Andreev processes) [12]; thus model-independent deconvolution cannot be performed since there are contributions from both normal and anomalous parts of the Green's function. In addition, the presence of the probing electrode (whether normal state or superconducting) induces some extrinsic broadening that needs to be subtracted out [12,16]. It is, however, possible to proceed in the other direction: assuming a specific model, one can compute the spectral function and then determine the differential conductance through integration. There is, however, a lack of theoretical works on the intrinsic temperature dependence of impurity spectra. Thermal effects are commonly added through phenomenological parameters by assuming certain relaxation rates or specific forms of the superconductor density of states (Dynes parameter for

smearing the coherence peaks), but little is known about quantitative behavior of microscopic models. The reasons are technical, as will be discussed at length in a later section of this paper. This work represents an attempt using the numerical renormalization group and achieves qualitative understanding of the intrinsic subgap temperature dependence due to electron-electron (*e-e*) interaction on the impurity site, while there are still significant quantitative systematic errors.

In this work we study the subgap spectral features in the single-impurity Anderson model with a superconducting bath described by the *s*-wave BCS mean-field Hamiltonian. After introducing the model and methods in Sec. II, with an emphasis on the technical challenges, we first consider the model by fixing the gap parameter Δ to its zero-temperature value and increasing the temperature T in Sec. III. This simplified calculation uncovers how the spectral weight is transferred from the subgap δ peak to the continuum. In this section we also study the hybridization and impurity level dependence and the differences between the singlet (screened impurity) and doublet (unscreened impurity) regimes. In Sec. IV we perform a full calculation with the temperature-dependent gap of a BCS superconductor; in this case the subgap peak broadening is accompanied by peak shifts. We conclude with a discussion of the possible experimental relevance of the results.

II. MODEL AND METHOD

We consider the Hamiltonian $H = H_{\mathrm{BCS}} + H_{\mathrm{imp}} + H_{\mathrm{c}}$:

$$H_{\mathrm{BCS}} = \sum_{k\sigma} \epsilon_k c_{k\sigma}^\dagger c_{k\sigma} - \Delta \sum_k (c_{k\uparrow}^\dagger c_{k\downarrow}^\dagger + \mathrm{H.c.}),$$

$$H_{\mathrm{imp}} = \epsilon_d \sum_\sigma n_\sigma + U n_\uparrow n_\downarrow, \qquad (1)$$

$$H_{\mathrm{c}} = \sum_{k\sigma} V_k (c_{k\sigma}^\dagger d_\sigma + \mathrm{H.c.}).$$

Here $c_{k\sigma}$ and d_σ are the band and impurity electron annihilation operators, ϵ_k is the band dispersion relation, Δ is the BCS gap parameter, ϵ_d is the impurity level, U is the *e-e* repulsion, $n_\sigma = d_\sigma^\dagger d_\sigma$ is the impurity occupancy operator, and V_k are the hopping integrals. The Hamiltonian does not include any coupling to electromagnetic noise or phonons since we focus on intrinsic subgap-state broadening due to local intraimpurity interaction effects.

Assuming a flat band with the density of states ρ in the normal state and $V_k \equiv V$, the impurity coupling is fully characterized by the hybridization strength $\Gamma = \pi \rho V^2$. The Kondo exchange coupling at the particle-hole symmetric point $\epsilon_d = -U/2$ and for $\Delta = 0$ is given by the Schrieffer-Wolff transformation as $\rho J_K = 8\Gamma/\pi U$, and the Kondo temperature is [17]

$$T_K^0 \sim U \sqrt{\rho J_K} \exp\left(-\frac{1}{\rho J_K}\right). \qquad (2)$$

In the superconducting case with $\Delta \neq 0$, the ground state of the system is either a singlet $|S\rangle$ or a doublet $|D\rangle$ depending on the value of the ratio Δ/T_K^0. All other eigenstates are, in the first approximation (i.e., neglecting residual interactions between the quasiparticles), product states of either $|S\rangle$ or $|D\rangle$ with additional Bogoliubov quasiparticles from the continuum.
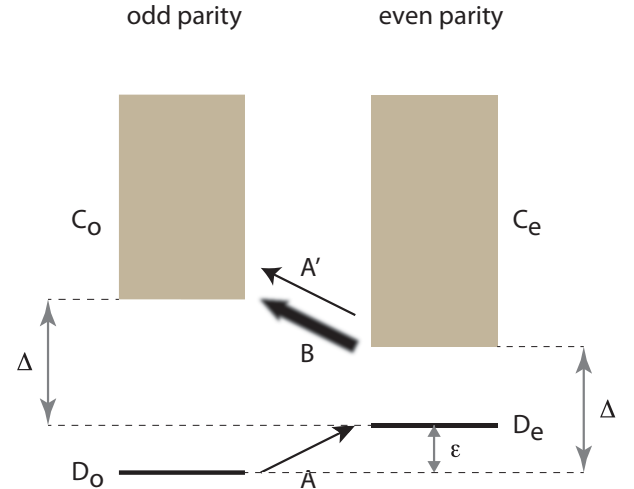

FIG. 1. Schematic diagram of the many-particle eigenstates of the Hamiltonian, partitioned into the even- and odd-fermion-parity sectors (i.e., with respect to the parity of the total electron number). This diagram corresponds to the case where the ground state has odd fermion parity (spin doublet). D_o and D_e are the odd-parity (spin-doublet) $|D\rangle$ and the even-parity (spin-singlet) $|S\rangle$ discrete eigenstates. The even-parity continuum C_e starts at energy Δ above the odd-parity discrete state D_o since the bottommost states of the continuum are composed of one additional quasiparticle added to D_o, thus changing the overall fermion parity. The odd-parity continuum C_o starts at energy Δ above the even-parity discrete state D_e for similar reasons. Labels A and A' indicate sharp transitions with $\omega = \epsilon$ (contributing to the subgap δ peak in the impurity spectrum), and the label B indicates diffuse transitions with $\omega \neq \epsilon$ (generating the continuous background in the spectrum). A corresponds to the transition between the many-particle states below the continuum edge, while A' form a set of similar transitions in the presence of a thermally excited quasiparticle, but totally elastic as far as the quasiparticles are concerned. In the absence of electron-electron interaction, there are no B transitions. Multiple-quasiparticle states are not shown; they start at 2Δ above D_o.

While the total particle number is not a conserved quantum number for $\Delta \neq 0$, its parity is. The eigenstates can thus be classified into odd- and even-fermion-parity sectors, as illustrated for the case of an odd-parity (spin-doublet) ground state in Fig. 1. A quasiparticle is an object with odd fermion parity; thus the even-parity continuum starts at the energy Δ above the odd-parity ground state, while the odd-parity continuum starts at the energy $\epsilon + \Delta$ above the ground state, where ϵ is the subgap-state "energy," more precisely, the energy difference

$$\epsilon = |E_S - E_D| \qquad (3)$$

between the subgap many-particle Shiba states.

In this work we are interested mainly in the spectral functions at finite T. The calculations are performed with the numerical renormalization group (NRG) [3,16,18–24]. This method appears at first perfectly suited for the problem since it is an unbiased nonperturbative numerical technique, applicable at both zero and finite temperatures, which can handle an arbitrary bath density of states (including with a superconducting gap), and provides the spectral function

directly on the real-frequency axis. Other methods are either biased, perturbative, inapplicable to the superconducting case, or require an analytical continuation from the Matsubara axis to real frequencies; in particular, this last issue makes the quantum Monte Carlo (QMC) approach of little use since it is extremely difficult to perform an analytical continuation in the presence of a sharp gap, especially since it is necessary (see below) to resolve a δ peak superposed on a continuous background of finite support inside the gap. Nevertheless, the situation under study in this work is in some regards perhaps the worst possible case for the NRG. While the method works very well for problems with a spectral gap at zero temperature and for nongapped baths at any temperature, there are severe difficulties when both Δ and T are nonzero. Both the gap and the temperature break the scale invariance on which the method is based, and they do so in different ways, thereby generating inevitable systematic errors. The results for spectral functions presented in this work should thus be considered as *qualitatively correct*, while quantitative errors are estimated (by monitoring how the results fluctuate when the NRG calculation parameters are varied) to be in the tens of percent range for $T \sim \Delta$. In spite of this major shortcoming, there is presently no other impurity solver to meaningfully study the finite-temperature spectral function in this problem. Static properties, such as the expectation values of various operators, can be reliably computed using the QMC [13,25]. Even here, there are some small systematic discrepancies between the QMC and NRG when *both* Δ and T are nonzero. Such comparisons of static properties are very useful to tune the parameters of the NRG to the values where such discrepancies are minimal. Finally, we note the fortunate fact that the finite-temperature problems in the NRG become severe when U is small, while they seem to be more manageable in the deep Kondo regime which is of main interest in this study.

The NRG calculations were performed with the discretization parameter $\Lambda = 2$, with $N_z = 8$ interleaved discretization grids [26,27], using the full-density-matrix algorithm with the Wilson chain terminated at the energy scale $E_{\text{chain}} = \Delta/50$ [28–30]. The "traditional" choice of the discretization parameter $\Lambda = 2$ proved to be near optimal. The results depend little on the choice of the discretization method [27]. The length of the Wilson chain, however, turned out to be a critical parameter and had to be tuned. To obtain a good description of the continuum part of the subgap spectrum at finite temperatures, it furthermore proved crucial to keep a large number of states in the NRG iteration even at energy scales below Δ, much more than required for obtaining well-converged thermodynamics and $T = 0$ spectral functions; we kept at least 2500 multiplets. While computationally demanding, this is critically important for a good description of the continuum quasiparticle spectrum in both the even- and odd-parity parts of the full Fock space [31].

The impurity Green's function is defined as

$$G(t) = -i\theta(t)\text{Tr}\{\rho[d_\sigma(t),d_\sigma^\dagger(0)]_+\}, \qquad (4)$$

where the trace is evaluated with the grand-canonical density matrix $\rho = e^{-\beta H}$ (the chemical potential is fixed to $\mu = 0$). This is an appropriate description only for well-equilibrated ergodic systems. The assumption of ergodicity is nontrivial

and may not be valid in all impurity systems and under all experimental conditions. Furthermore, the presence of the tunneling contacts will drive the system out of equilibrium.

The impurity spectral function,

$$A(\omega) = -\frac{1}{\pi}\text{Im}\tilde{G}(\omega + i\delta), \qquad (5)$$

where $\tilde{G}$ is the Fourier transform of G, can be expressed using the Lehmann decomposition as

$$A(\omega) = \frac{1}{Z}\sum_{mn}|\langle m|d_\sigma|n\rangle|^2$$
$$\times (e^{-\beta E_m} + e^{-\beta E_n})\delta(\omega + E_m - E_n), \qquad (6)$$

where m,n index all eigenstates of the Hamiltonian, $E_{m,n}$ are the corresponding eigenvalues, $\beta = 1/k_B T$, and the grand-canonical partition function is $Z = \text{Tr}[\exp(-\beta H)] = \sum_m \exp(-\beta E_m)$. The actual calculation of $A(\omega)$ is performed using the full-density-matrix algorithm [30], generalizing the complete-Fock-space approach [28,29], which has a significantly more complex Lehmann-like spectral decomposition. We accumulate the raw spectral data separately for $|\omega| < \Delta$ and $|\omega| > \Delta$. Inside the gap, we use 5000 equidistant bins. Outside the gap, we use a logarithmic mesh of bins with low-frequency accumulation points at $\omega = \pm\Delta$ and with 1000 bins per frequency decade. This modification of the standard binning is necessary for obtaining constant spectral resolution inside the gap and a correct description of the gap edges in the continuum above the gap [32].

The Green's function probes the single-particle excitations of the system. It should be emphasized that all contributions to G correspond to electron-parity-changing transitions (see Fig. 1). Let us consider the doublet regime, where the impurity spin is unscreened and the ground state is the odd-parity spin doublet $|D\rangle$. At zero temperature, only the ground state D_o is thermally occupied, and the only transition with $\Delta E < \Delta$ is that to the discrete excited state D_e (transition A indicated by the sharp arrow in Fig. 1). The subgap part of the spectrum is thus fully described by two δ peaks at positions $\omega = \pm\epsilon$ with equal weight (at the particle-hole symmetry) given by

$$W_\delta(T = 0) = \tfrac{1}{2}|\langle D_o|d_\sigma|D_e\rangle|^2. \qquad (7)$$

At finite temperatures there are further transitions with starting and end states separated by less than Δ: they are indicated by the arrow labeled A' (representing an infinite set of transitions with exactly $\omega = \epsilon$) and a diffuse arrow B in Fig. 1. They correspond to transitions from the thermally populated even-parity quasiparticle states at energies above Δ (set C_e) to the odd-parity quasiparticle states at energies above $\epsilon + \Delta$ (set C_o). The set A' corresponds to perfectly elastic processes and also contributes in the absence of interaction U, while the set B corresponds to inelastic exchange scattering of quasiparticles and is due to the electron-electron interaction on the impurity site. Since the states involved in B form continua, this will generate a continuous spectral weight contribution to the subgap spectrum. The most likely transitions are those from the bottom of C_e to the bottom of C_o; thus the continuum background is expected to be peaked at $|\omega| = \epsilon$, i.e., at the position of the discrete subgap state, which itself persists at finite temperature at least up to $T \sim \Delta$. The evolution

with increasing T is thus expected to be as follows: the weight of the δ peak decreases, while the weight of a new broad peak centered at the same position increases. In the next sections, we confirm this intuitive physical picture by numerical calculations.

At finite temperatures some care is required in postprocessing the raw spectral data as obtained from the NRG run. The δ peak is extracted from the spectral function by removing the weight in a narrow interval of width $2 \times 10^{-4}\Delta$ around $\omega = \epsilon$, where ϵ can be independently determined very accurately from the NRG flow diagrams. The results remain essentially unchanged upon further narrowing of the interval. The remaining continuous part of the spectral function is then broadened and further characterized. This procedure allows us to reliably partition the spectral function into discrete and continuous components:

$$A(\omega) = A_\delta(\omega) + A_c(\omega). \tag{8}$$

The corresponding spectral weights are defined as

$$W_i = \int_0^\Delta A_i(\omega)\,d\omega, \tag{9}$$

with $i = \delta, c$. It should be noted in passing that at finite temperatures $W_\delta(T)$ receives contributions not only from the transition A but also from a discrete subset of transitions between the states forming the continua C_e and C_o with energy difference *exactly* equal to ϵ (i.e., the transitions $D_e \to D_o$ in the presence of quasiparticles, but without the quasiparticles interacting with the impurity). The temperature dependence of both W_δ and W_c is an interaction effect: for a noninteracting Hamiltonian, such as that corresponding to a classical impurity with no internal dynamics, the spectral function itself would not depend in any way on the temperature (although the *occupancies* of the single-particle levels would change with T).

III. RESULTS: FIXED Δ

A. Overview and main characteristics

The calculations in this section are performed for fixed model parameters ($\Gamma/U = 0.1$, $\epsilon_d = -U/2$, $U/\Delta = 20$); only the temperature T is varied. The ground state is a spin doublet, while the singlet excited state lies at the energy level

$$\epsilon = 0.423\Delta \tag{10}$$

above it. Due to the particle-hole (p-h) symmetry the spectral function is even, and we focus on its $\omega > 0$ (particle addition) part. At zero temperature, the weight of the δ peak at $\omega = \epsilon$ is

$$W_\delta(T = 0) = 0.0341. \tag{11}$$

This indicates that the Shiba bound state wave function (as far as it can be defined for an interacting system) has the majority of its weight not in the impurity but in the host, which is commonly the case for Shiba states.

The most important spectral characteristics are revealed in the temperature-dependence plots shown in Fig. 2, while an example of a typical finite-T spectral function is shown in Fig. 3. Since the continuum part needs to be obtained by broadening raw results in the form of a sum of δ peaks, its
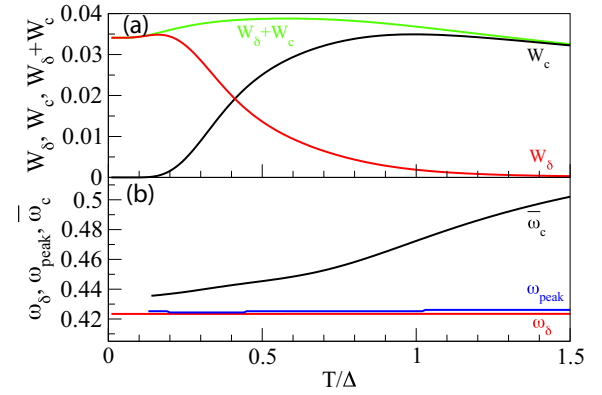

FIG. 2. (a) δ peak, continuum, and total spectral weight W in the positive-frequency subgap part ($0 < \omega < \Delta$) of the impurity spectral function $A(\omega, T)$. (b) Positions of the δ peak, ω_δ, and of the maximum of the continuous part, ω_{peak}, as well as the mean value of the continuous part $\bar{\omega}_c$.

appearance depends on the choice of the kernel width. Here the kernel is chosen sufficiently narrow to reduce overbroadening effects at the price of small artifacts which are unphysical. Thus the asymmetry of the continuum is a real feature; the secondary peak is most likely an artifact of the method. For this reason it is more meaningful to discuss the spectral moments rather than the detailed shape of the spectrum.

The continuum weight W_c exhibits activated behavior for low T, with the activation energy Δ:

$$W_c(T) = 0.168\,e^{-\Delta/T}. \tag{12}$$

This confirms the expectation that the continuum background is associated with the *inelastic* transitions that require a finite thermal population of the quasiparticle states above the gap which scatter on the impurity (diffuse transitions as shown schematically in Fig. 1, arrow B).
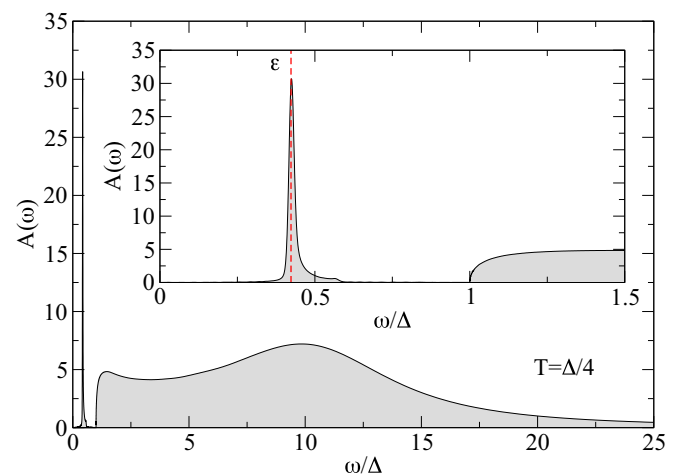

FIG. 3. Impurity spectral function $A(\omega, T)$ at finite temperature $T = \Delta/4$. The hump at $\omega = 10\Delta = U/2$ is the Hubbard peak. The inset shows a close-up of the subgap region. The position of the δ peak ϵ is indicated using the dashed line and almost coincides with the peak of the continuum part.

For $T \gtrsim 0.2\Delta$, W_δ is a strictly decreasing function of temperature, while W_c is increasing, and their sum $W_\delta + W_c$ is approximately constant: the weight is gradually transferred from the coherent discrete subgap state to diffuse states involving itinerant quasiparticle states; this represents a thermal decomposition of the Shiba state. We note that $W_\delta = W_c$ on the scale $T \approx \Delta/2$. This is also the range where the total weight $W_\delta + W_c$ reaches a maximum value. The continuum weight W_c is increasing up to $T \approx \Delta$, where it reaches a value close to $W_\delta(T = 0)$. In simple terms, with increasing temperature almost all spectral weight is transferred from the δ peak to the continuum by $T \approx \Delta$. For $T > \Delta$, W_c itself becomes a decreasing function, albeit only weakly: the decay of W_δ at large T is much faster than that of W_c, and W_δ becomes essentially zero by $T \approx 2\Delta$.

In Fig. 2(b) we consider the peak positions. The δ peak does not move with temperature. This is expected since its position $\omega_\delta = \epsilon$ is given by the energy difference between two discrete eigenstates of the Hamiltonian; thus it is a property of the operator itself and does not involve any thermal effects. The continuum part of the subgap spectrum is a peaked function (see Fig. 3). The position of this peak ω_{peak} almost coincides with the δ-peak position,

$$\omega_{\text{peak}} \approx \omega_\delta = \epsilon, \qquad (13)$$

since the main contribution comes from processes linking the bottommost part of both continua. Interestingly, ω_{peak} is very weakly temperature dependent even at T of order Δ. We also plot the mean of the continuum part $\bar{\omega}_c$, defined as the normalized first moment of $A_c(\omega)$. The mean is larger than ϵ and further increases with T, indicating that the continuum part of the spectrum is skewed toward larger frequencies, as can also be seen in Fig. 3. At low temperatures, the skewness exceeds 6 and is thus significant. The long tail is due to the asymmetry of the transitions: the most populated thermally excited starting states are those near the bottom of the even-parity continuum, and the most likely end states are those at the bottom of the odd-parity continuum starting at ϵ higher in energies. At higher temperatures, $T \sim \Delta$, the distribution becomes more symmetric around $\omega = \epsilon$ with a clear dominant peak, corresponding to the "thermally broadened" subgap resonance.

The width of the continuum part can be further characterized through the standard deviation σ_c (see Fig. 4). It is a strictly increasing function of T. At intermediate temperatures $T \approx \Delta/2$ it reaches a value of order 0.1Δ; thus the background is relatively broad. Another relevant quantity is the half width at half maximum (HWHM) of the main peak in the continuum part. Unfortunately, this quantity is very difficult to extract reliably since it requires a delicate broadening procedure and
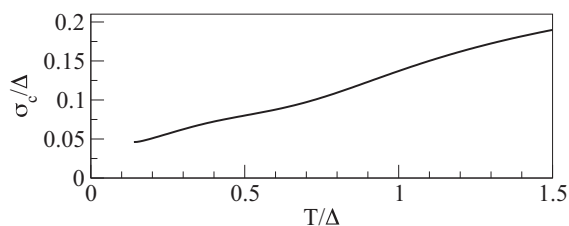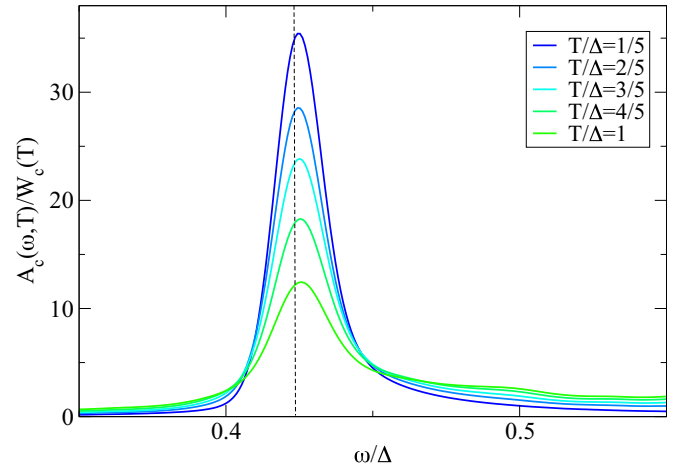

FIG. 5. Temperature dependence of the continuum part of the subgap spectrum $A_c(\omega, T)$. The spectra are normalized by dividing by the total weight of the continuum contribution $W_c(T)$, shown in Fig. 2(a).

it strongly depends on the NRG calculation parameters; thus the extracted values are quantitatively unreliable. We find that the HWHM is only weakly increasing in the temperature range $T < \Delta$: it starts at values close to 0.01Δ in the low-temperature limit and increases to $\sim 0.015\Delta$ at $T = \Delta$. The significant difference between the standard deviation and the HWHM is consistent with $A_c(\omega)$ being a long-tailed skewed distribution.

We now take a closer look at the redistribution of the continuum weight at increasing temperature by plotting $A_c(\omega, T)/W_c(T)$, i.e., the continuum subgap spectrum renormalized by the total continuum weight W_c (see Fig. 5). The spectrum always has a single dominant peak with the maximum close to ϵ and with a long tail extending toward high frequencies. As T increases, the weight redistributes from the main peak to the wider subgap frequency range; thus the system becomes increasingly incoherent.

B. Γ dependence

We now study how the results from the previous section depend on the value of the hybridization Γ, in particular across the singlet-doublet quantum phase transition where $|S\rangle$ and $|D\rangle$ interchange their roles as the ground and the excited states, respectively.

For low enough Γ, so that the impurity is in the Kondo regime, the Shiba state energy ϵ follows the universal dependence $\epsilon(T_K/\Delta)$, where $T_K = T_K(\Gamma)$. For $\Gamma \to 0$, the peak is close to the gap edge; then it moves toward the chemical potential for increasing Γ (see Fig. 6). For chosen $U/\Delta = 20$, the singlet-doublet (S-D) transition occurs at

$$\Gamma_c = 0.155U. \qquad (14)$$

We first consider how the temperature dependencies of the key spectral characteristics change for different values of Γ. The δ-peak position $\omega_\delta = \epsilon$ does not vary with temperature. The continuum mean ω_c, shown in Fig. 7, starts from $\omega_c(T = 0) \approx \epsilon$ for $\Gamma < \Gamma_c$, while for $\Gamma \gtrsim \Gamma_c$ it starts from values close to the gap edge (this peculiar low-temperature behavior will be
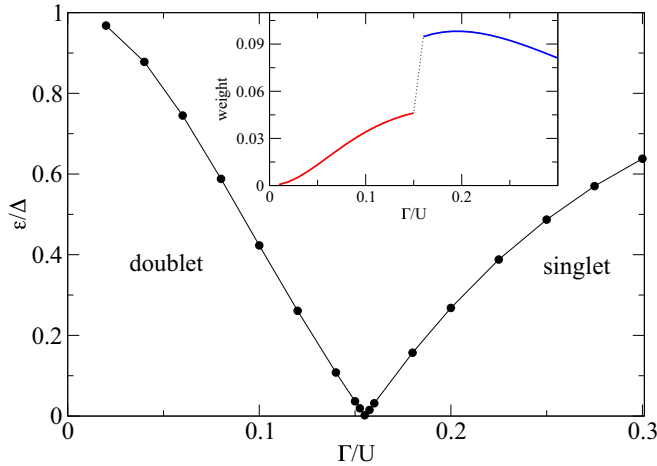

FIG. 4. Width (standard deviation) of the continuum part.

FIG. 6. Subgap-state energy ϵ as a function of the hybridization strength Γ for fixed $U/\Delta = 20$. The inset shows the $T = 0$ spectral weight of the subgap δ peak.

explained in Sec. III D). In the temperature range $T \lesssim \Delta$, ω_c is a decreasing function of T for all cases where ϵ is close to the gap edge (i.e., in deep doublet and in deep singlet phases), while it is nonmonotonic or increasing for $\epsilon \ll \Delta$ (i.e., in the transition range with Shiba states deep in the gap; see Fig. 7).

The continuous-background weight W_c is strictly increasing as a function of Γ at any fixed T up to

$$\Gamma^* \approx 0.225U \tag{15}$$

(see Fig. 8). For $\Gamma \lesssim \Gamma^*$, the system is in the regime of well-defined local moment (the Hartree-Fock solution spin polarizes for $\Gamma < U/\pi \approx 0.3U$) with properties controlled by the ratio Δ/T_K, while for $\Gamma \gtrsim \Gamma^*$ the charge fluctuations are important and the impurity properties become nonuniversal. At low T, the same exponential law $W_c = be^{-\Delta/T}$ is found
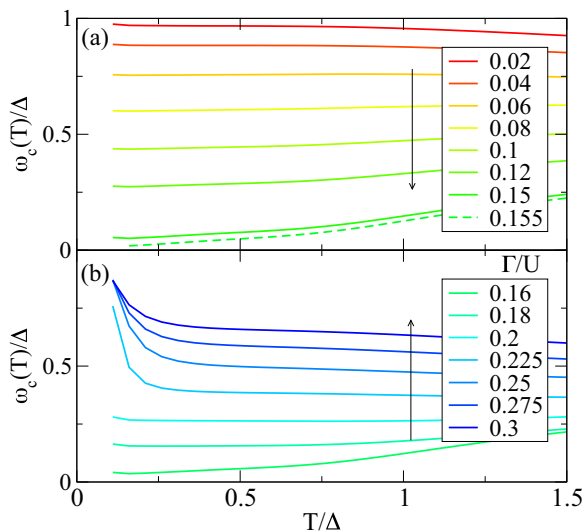

FIG. 7. Temperature dependence of the mean value of the continuum part of the subgap spectrum $\omega_c(T)$ for a range of hybridization strengths Γ in (a) doublet and (b) singlet regimes. The arrow indicates the direction of increasing Γ.
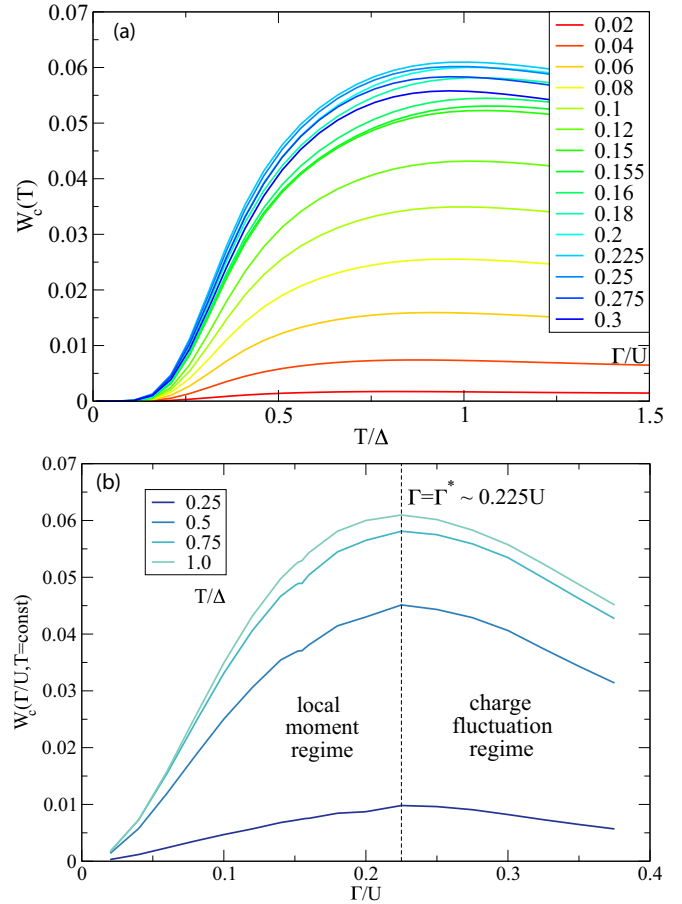

FIG. 8. (a) Temperature dependence of the continuum-part weight $W_c(T)$ for a range of hybridization strengths Γ. (b) Γ dependence for a range of fixed temperatures.

for all values of $\Gamma \lesssim \Gamma^*$, both in the singlet and in the doublet regimes, with $b(\Gamma)$ dependence, which can be read off from Fig. 8(b). For $\Gamma \gtrsim \Gamma^*$, however, we find some deviations from pure exponential dependence. The maximum in $W_c(T)$ is always on the scale $T \sim \Delta$.

The δ-peak weight is monotonically decreasing as a function of T for small Γ and has a local maximum for intermediate $\Gamma < \Gamma_c$ (see Fig. 9). The temperature of the maximum shifts to lower temperatures as Γ increases toward Γ_c, and for $\Gamma > \Gamma_c$ the weight again becomes a monotonically decreasing function of T. This pronounced difference in the low-T regime for $\Gamma \approx \Gamma_c$ can serve as a tool to distinguish between the doublet and singlet regimes at finite temperatures. Indeed, in the zero-temperature limit and in the absence of magnetic field (as assumed throughout this work) the subgap weight changes discontinuously by a factor of 2 across the S-D transition (see the inset in Fig. 6). At finite T, this discontinuity is washed out (see the inset in Fig. 9). The upturn/downturn of $W_\delta(T)$ occurs at $T \approx |\epsilon|$, and this scale moves toward zero as $\Gamma \to \Gamma_c$, as shown in the main panel of Fig. 6.

For $\Gamma > \Gamma^*$ the charge fluctuations lead to a decreasing subgap spectral weight. The decreasing trend is also related to the fact that the δ peak moves close to the gap edge in the limit $\Gamma \gg \Gamma^*$. This is a known effect: subgap states merge with the continuum in a continuous way by transferring spectral weight
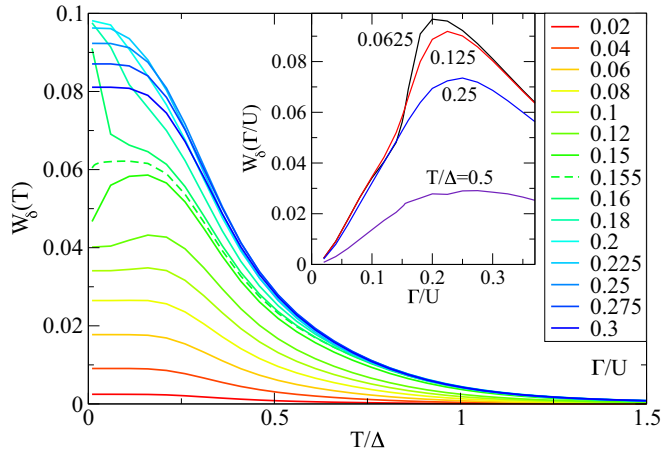
FIG. 9. Temperature dependence of the δ-peak weight $W_\delta(T)$ for a range of hybridization strengths Γ. Inset: Γ dependence of $W_\delta(T)$ at finite temperature, which should be compared with the inset in Fig. 6 showing the same quantity at $T = 0$.

FIG. 11. Subgap spectrum for strong hybridization $\Gamma = 0.3U$. The inset shows the temperature dependence of the weight and position of the secondary peak which appears just below the gap edge.

from the δ peak to the quasiparticle part, so that the weight of the δ peak goes to zero as its position approaches $\omega = \Delta$.

C. ϵ_d dependence

The singlet-doublet transition can also be induced by moving away from the p-h symmetric point by changing the impurity level ϵ_d from the value $-U/2$. The spectral function is then no longer an even function of frequency. The temperature dependence of the weights is shown in Fig. 10 for two values on either side of the transition point. The temperature variation of the total subgap spectral weight is
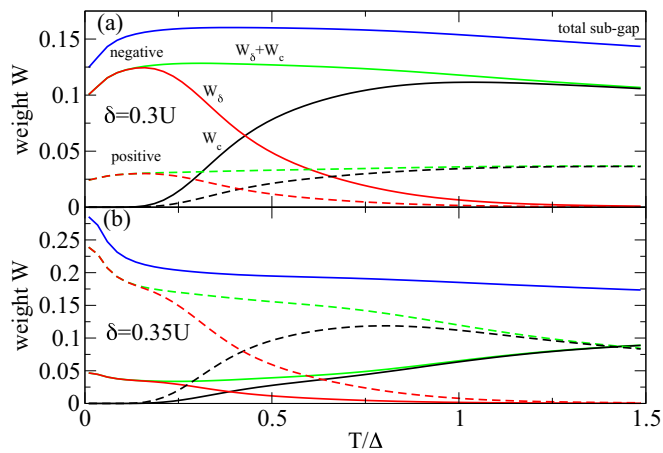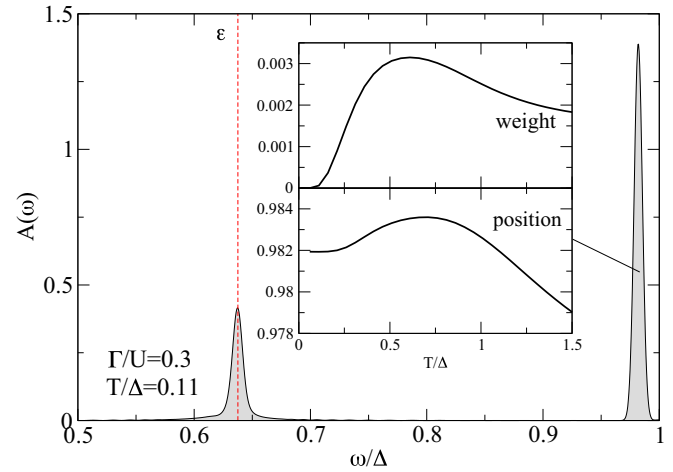

FIG. 10. Temperature dependence of the subgap spectral weight away from the particle-hole symmetric point. We plot separately the negative frequency part (solid lines) and the positive part (dashed lines), further separated into δ-peak and continuum contributions. Here $\delta = \epsilon_d + U/2$ is a parameter which measures the departure from the particle-hole symmetric point. We plot two cases close to the singlet-doublet transition point: (a) doublet ground state ($\epsilon = 0.062\Delta$) and (b) singlet ground state ($\epsilon = 0.12\Delta$). Note the change of the dominant peak from the negative to positive side across the phase transition.

significant in this regime due to the low excitation energy ϵ and because the two subgap states correspond to different expectation values of the impurity occupancy [33,34]; hence $\langle n \rangle(T)$ has activated behavior with the activation energy ϵ. In regard to the transfer of spectral weight from the δ peaks to the continuous background, we find results similar to those in the p-h symmetric case, with $\exp(-\Delta/T)$ behavior and crossing of the curves at $T \approx \Delta/2$.

For even larger $\delta = \epsilon_d + U/2 \approx 0.45U$, well in the valence fluctuation regime, we observe anomalies in the spectral means at low temperatures similar to those for large Γ.

D. Anomalies for large Γ

Several anomalies are observed for large values of Γ and for impurity level ϵ_d far away from the particle-hole symmetric point. Their common origin is an additional subgap spectral peak just below the gap edge (see Fig. 11). The weight of this peak shows activated behavior at low temperatures:

$$w_2(T) = 0.018 e^{-\epsilon/T}, \tag{16}$$

where $\epsilon = 0.637\Delta$ for the chosen value $\Gamma/U = 0.3$. This peak dominates the continuum background for small T because its activation energy ϵ is lower than that (Δ) of the continuous background centered around the subgap peak. The dominance of the additional peak in the low-T limit explains the strikingly peculiar low-T behavior of $\omega_c(T)$ in Fig. 7. Extensive testing has been performed to see if this feature could be merely a numerical artifact of the NRG method. Varying Λ, the Wilson chain length, the discretization scheme, the algorithm for computing the spectral function (naive Lehmann-decomposition approach, complete Fock space, full density matrix), and the number of states kept in the truncation, it was found that this feature persists. It is thus either a generic artifact of the method for finite T and Δ that cannot be eliminated by any parameter choice or a real spectral feature of the Anderson impurity model with superconducting baths. Presently, there is no other theoretical method to reliably confirm the presence of this
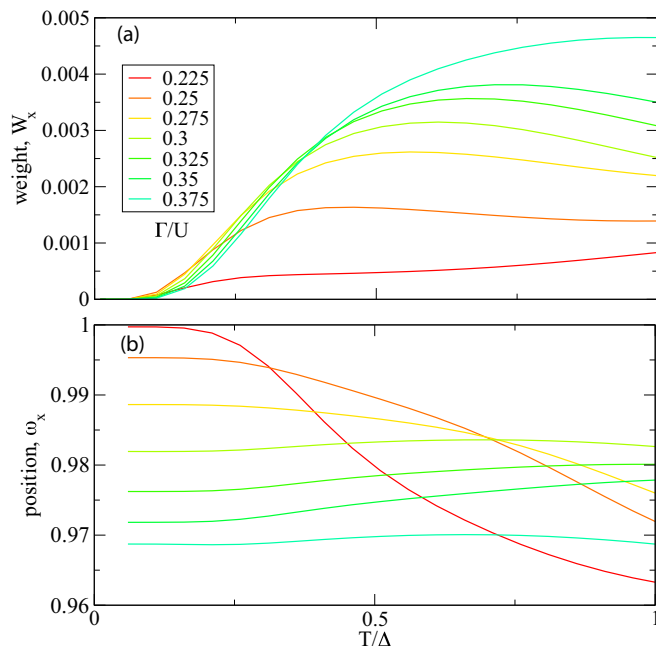
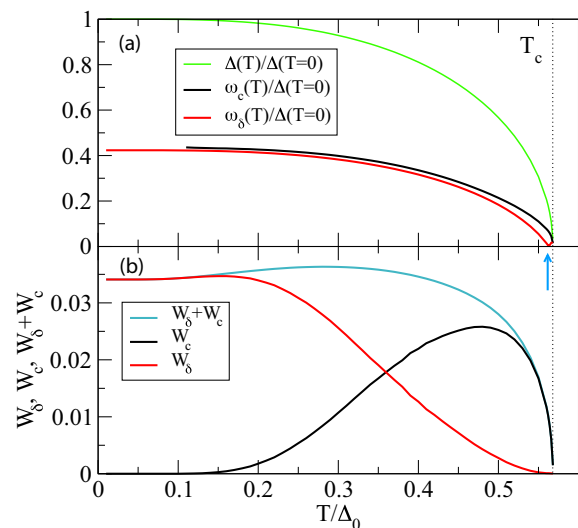FIG. 12. (a) Weight and (b) position of the weakly bound additional resonance just below the gap edge.

FIG. 13. Temperature dependence of the quantities characterizing the subgap spectral function in the case of $\Delta = \Delta_{\text{BCS}}(T)$. The temperature-driven doublet-singlet phase transition is indicated by the arrow. Model parameters are $\Gamma/U = 0.1$ and $U/\Delta \approx 20$.

peak. However, the spectral weight appears sufficiently large that it could be detected experimentally, despite its vicinity to the gap edge.

It should be emphasized that there are no discrete subgap multiparticle states with the energy corresponding to this peak. Instead, its origin is associated with quasiparticle scattering on the *thermally* excited doublet subgap state $|D\rangle$ (for large Γ and far away from the particle-hole symmetric point, the ground state is $|S\rangle$), generating new bound states of Bogoliubov quasiparticles.

Figure 12 shows the dependence of the weight and position of the additional peak. The threshold for the existence of the peak is related to Γ^*; thus the peak is intimately related to entering the charge-fluctuation regime. Close to the threshold, its $T = 0$ position is at the gap edge, while for larger Γ it starts at a finite binding energy below the edge.

IV. RESULTS: BCS $\Delta(T)$

We now consider a realistic case where the gap Δ is temperature dependent and tends to zero as the critical temperature T_c is approached. We use a simplified phenomenological expression

$$\Delta_{\text{BCS}}(T) \approx \delta_{sc} T_c \tanh\left[\frac{\pi}{\delta_{sc}}\sqrt{a\frac{\delta C}{C_N}\left(\frac{T_c}{T} - 1\right)}\right], \quad (17)$$

with $\delta_{sc} = 1.76, a = 2/3, \delta C/C_N = 1.43$, which is a good approximation for the true BCS temperature dependence with correct $T \to 0$ and $T \to T_c$ asymptotics.

We consider the case where the system is in the doublet regime at $T = 0$. The temperature dependence of key quantities is shown in Fig. 13. The reduction of Δ with increasing T drives the system toward the singlet regime. The doublet-singlet transition occurs, however, just before

the critical point (indicated by the arrow in the figure). The variation of the weights is quite similar to that in the fixed-Δ calculation [compare Figs. 2(a) and 13(b)].

V. DISCUSSION

Based on general considerations of an interacting impurity system and confirmed by numerical calculations, Shiba states at finite temperature lose spectral weight to a continuous subgap background centered at the same position. This immediately leads to a question of principle about the proper definition of the intrinsic lifetime of a subgap state. A discrete excited many-particle state isolated from the continuum could be expected to not decay at all. This is clearly the case in the absence of quasiparticles. In an open system at finite temperature, i.e., in contact with a heat and particle reservoir, a quasiparticle in the superconductor can be generated through a thermal fluctuation and can interact with the impurity spin, giving rise to a continuum background. The excited subgap many-particle state can release its excitation energy to the incident quasiparticle and decay to the many-particle ground state, resulting in a finite lifetime.

The model system studied here is admittedly simplistic. In realistic systems, in particular when there are tunneling pathways to a normal metal (such as a normal-state tip of a scanning tunneling microscope), the δ peak will, strictly speaking, no longer exist. Similarly, (direct or indirect) coupling to the acoustic phonons of the host will broaden the δ peak. If such couplings are small, however, it may still be expected that the impurity spectral function could be multimodal with nontrivial temperature dependence. For large couplings, the details cannot be observed, and intrinsic lifetime due to *e-e* interaction would be merely a correction to the total width with the main contribution arising from other processes.

Let us now consider the example of Mn adatoms on Pb(111) studied in Ref. [12]. Pb has $\Delta(T = 0) \approx 1.35$ meV.

The experimental temperatures of $T_1 = 1.2$ K and $T_2 = 4.8$ K correspond approximately to $k_B T/\Delta$ of 0.07 and 0.33, respectively. The most pronounced Shiba state occurs at $\epsilon/\Delta(T = 0) = 0.16$. T_1 corresponds to the low-T limit, while at T_2 the finite-temperature effects are expected to be sizable. At T_1 the measured linewidth was resolution limited and had to be estimated indirectly through current saturation plateaus, yielding $\Gamma = \hbar/0.8$ ps $< 1\,\mu$eV. At T_2, the width can be extracted from the peak width in the weak-coupling regime, giving $\Gamma \approx \hbar/6$ ps ≈ 0.11 meV. Thus $\Gamma/\Delta(T = 0) \approx 0.1$. In order to estimate what proportion of this total relaxation rate could originate from the intrinsic *e*-*e* processes, we have performed a calculation for the Anderson impurity model with parameters tuned so that the Shiba state energy corresponds to the dominant Shiba peak from the experiment ($\Gamma/U = 0.133, U/\Delta = 20$, giving $\epsilon/\Delta \approx 0.16$). The differential conductance has been computed at the same level of approximation as in Ref. [12], but using the Green's function matrix obtained from the NRG calculation. The result of such a calculation at the temperature matching T_2 is shown in Fig. 14. Peak widths were estimated by fitting Fano resonance line shapes, which gives $\Gamma_{\mathrm{intr}} \approx 0.012\Delta$. While this value is model and parameter dependent even if ϵ/Δ and T/Δ are matched to those from the experiment, it is a useful order-of-magnitude estimate. We thus find that for this particular physical system, the contribution of the intrinsic electron-electron processes as described in a *single-orbital* Anderson impurity model is a minor contribution to the total value.

This work opens up a number of interesting issues for further study: Are there other systems where the phonon effects are smaller and the intrinsic width could be significant? Are the widths enhanced in multiorbital impurity models, perhaps
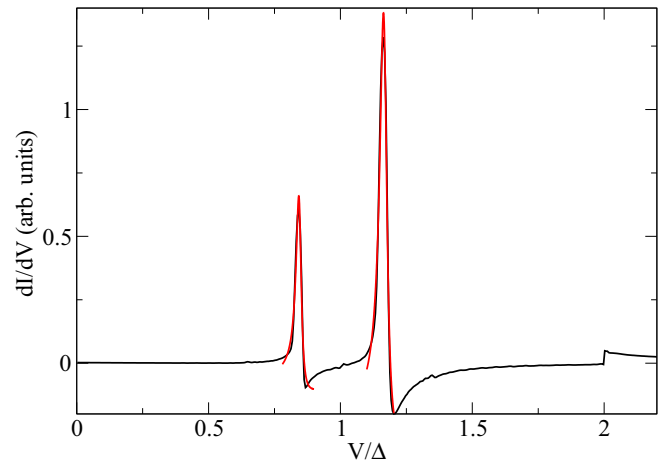

FIG. 14. Predicted differential conductance dI/dV based on the finite-temperature impurity Green's function from the NRG, calculated in the limit of weak tip-impurity coupling.

due to additional relaxation processes involving multiple Shiba states? How are the results modified if the BCS mean-field Hamiltonian is replaced by a proper interacting model with electron-electron attraction terms and the calculation is performed fully self-consistently? Finally, a better theoretical understanding of the additional thermally generated bound states and their relation to the charge fluctuations is needed.

ACKNOWLEDGMENTS

[1] H. Shiba, Classical spins in superconductors, Prog. Theor. Phys. **40**, 435 (1968).

[2] H. Shiba, A Hartree-Fock theory of transition-metal impurities in a superconductor, Prog. Theor. Phys. **50**, 50 (1973).

[3] K. Satori, H. Shiba, O. Sakai, and Y. Shimizu, Numerical renormalization group study of magnetic impurities in superconductors, J. Phys. Soc. Jpn. **61**, 3239 (1992).

[4] A. V. Balatsky, I. Vekhter, and J.-X. Zhu, Impurity-induced states in conventional and unconventional superconductors, Rev. Mod. Phys. **78**, 373 (2006).

[5] A. Yazdani, B. A. Jones, C. P. Lutz, M. F. Crommie, and D. M. Eigler, Probing the local effects of magnetic impurities on superconductivity, Science **275**, 1767 (1997).

[6] R. S. Deacon, Y. Tanaka, A. Oiwa, R. Sakano, K. Yoshida, K. Shibata, K. Hirakawa, and S. Tarucha, Interplay of Kondo and Superconducting Correlations in the Nonequilibrium Andreev Transport through a Quantum Dot, Phys. Rev. Lett. **104**, 076805 (2010).

[7] J.-D. Pillet, C. H. L. Quay, P. Morin, C. Bena, A. Levy Yeyati, and P. Joyez, Andreev bound states in supercurrent-carrying carbon nanotubes revealed, Nat. Phys. **6**, 965 (2010).

[8] R. Maurand, T. Meng, E. Bonet, S. Florens, L. Marty, and W. Wernsdorfer, First-Order 0-π Quantum Phase Transition in the Kondo Regime of a Superconducting Carbon-Nanotube Quantum Dot, Phys. Rev. X **2**, 011009 (2012).

[9] K. J. Franke, G. Schulze, and J. I. Pascual, Competition of superconductivity phenomena and Kondo screening at the nanoscale, Science **332**, 940 (2011).

[10] A. Martín-Rodero and A. Levy Yeyati, Josephson and Andreev transport through quantum dots, Adv. Phys. **60**, 899 (2011).

[11] A. Kumar, M. Gaim, D. Steininger, A. Levy Yeyati, A. Martín-Rodero, A. K. Hüttel, and C. Strunk, Temperature dependence of Andreev spectra in a superconducting carbon nanotube quantum dot, Phys. Rev. B **89**, 075428 (2014).

[12] M. Ruby, F. Pientka, Y. Peng, F. von Oppen, B. W. Heinrich, and K. J. Franke, Tunneling Processes into Localized Subgap States in Superconductors, Phys. Rev. Lett. **115**, 087001 (2015).

[13] D. J. Luitz and F. F. Assaad, Weak-coupling continuous-time quantum Monte Carlo study of the single impurity and periodic Anderson models with s-wave superconducting baths, Phys. Rev. B **81**, 024509 (2010).

[14] J.-D. Pillet, P. Joyez, R. Žitko, and M. F. Goffman, Tunneling spectroscopy of a single quantum dot coupled to a superconductor: From Kondo ridge to Andreev bound states, Phys. Rev. B **88**, 045101 (2013).

[15] M. Žonda, V. Pokorný, V. Janiš, and T. Novotný, Perturbation theory for an Anderson quantum dot asymmetrically attached to two superconducting leads, Phys. Rev. B **93**, 024523 (2016).

[16] R. Žitko, J. S. Lim, R. Lopez, and R. Aguado, Shiba states and zero-bias anomalies in the hybrid normal-superconductor Anderson model, Phys. Rev. B **91**, 045441 (2015).

[17] H. R. Krishna-murthy, J. W. Wilkins, and K. G. Wilson, Renormalization-group approach to the Anderson model of dilute magnetic alloys. I. Static properties for the symmetric case, Phys. Rev. B **21**, 1003 (1980).

[18] K. G. Wilson, The renormalization group: Critical phenomena and the Kondo problem, Rev. Mod. Phys. **47**, 773 (1975).

[19] O. Sakai, Y. Shimizu, H. Shiba, and K. Satori, Numerical renormalization group study of magnetic impurities in superco-ductors. II. Dynamical excitations spectra and spatial variation of the order parameter, J. Phys. Soc. Jpn. **62**, 3181 (1993).

[20] T. Yoshioka and Y. Ohashi, Numerical renormalization group studies on single impurity anderson model in superconductivity: A unified treatment of magnetic, nonmagnetic impurities, and resonance scattering, J. Phys. Soc. Jpn. **69**, 1812 (2000).

[21] A. Oguri, Y. Tanaka, and A. C. Hewson, Quantum phase transition in a minimal model for the Kondo effect in a Josephson junction, J. Phys. Soc. Jpn. **73**, 2494 (2004).

[22] J. Bauer, A. Oguri, and A. C. Hewson, Spectral properties of locally correlated electrons in a Bardeen-Cooper-Schrieffer superconductor, J. Phys. Condens. Matter **19**, 486211 (2007).

[23] C. Karrasch, A. Oguri, and V. Meden, Josephson current through a single Anderson impurity coupled to BCS leads, Phys. Rev. B **77**, 024517 (2008).

[24] R. Bulla, T. Costi, and T. Pruschke, The numerical renormal-ization group method for quantum impurity systems, Rev. Mod. Phys. **80**, 395 (2008).

[25] E. Gull, A. J. Millis, A. I. Lichtenstein, A. N. Rubtsov, M. Troyer, and P. Werner, Continuous-time Monte Carlo methods for quantum impurity models, Rev. Mod. Phys. **83**, 349 (2011).

[26] W. C. Oliveira and L. N. Oliveira, Generalized numerical renormalization-group method to calculate the thermodynam-ical properties of impurities in metals, Phys. Rev. B **49**, 11986 (1994).

[27] R. Žitko and T. Pruschke, Energy resolution and discretization artifacts in the numerical renormalization group, Phys. Rev. B **79**, 085106 (2009).

[28] F. B. Anders and A. Schiller, Real-Time Dynamics in Quantum Impurity Systems: A Time-Dependent Numerical Renormaliza-tion Group Approach, Phys. Rev. Lett. **95**, 196801 (2005).

[29] R. Peters, T. Pruschke, and F. B. Anders, A numerical renor-malization group approach to Green's functions for quantum impurity models, Phys. Rev. B **74**, 245114 (2006).

[30] A. Weichselbaum and J. von Delft, Sum-Rule Conserving Spectral Functions from the Numerical Renormalization Group, Phys. Rev. Lett. **99**, 076402 (2007).

[31] A possible improvement consists of formulating the NRG truncation rule so that a comparable total number of multiplets is kept in even- and odd-fermion-parity sectors, but this has not yet been tried out.

[32] T. Hecht, A. Weichselbaum, J. von Delft, and R. Bulla, Nu-merical renormalization group calculation of near-gap peaks in spectral functions of the Anderson model with superconducting leads, J. Phys. Condens. Matter **20**, 275213 (2008).

[33] R. Žitko, O. Bodensiek, and Th. Pruschke, Magnetic anisotropy effects on quantum impurities in superconducting host, Phys. Rev. B **83**, 054512 (2011).

[34] D. Golež, J. Bonča, and R. Žitko, Vibrational Andreev bound states in magnetic molecules, Phys. Rev. B **86**, 085142 (2012).